Geochemical Perspectives Letters



# Onset of volatile recycling into the mantle determined by xenon anomalies

**S. Péron, M. Moreira**

## Supplementary Information

The Supplementary Information includes:

- Material and Method
- Tables S-1 to S-2
- Figures S-1 to S-9
- Supplementary Information References

### *Material and Method*

#### Sample

Fresh, centimetre-sized glass pieces of popping rock 2πD43 sample (Bougault *et al.*, 1988; Sarda and Graham, 1990; Javoy and Pineau, 1991; Moreira *et al.*, 1998) were selected. This basaltic glass sample from the Mid-Atlantic Ridge (around 14 °N) has a huge vesicularity, around 16 % (Sarda and Graham, 1990), and so is very rich in noble gases, making it the best sample to test a protocol for accumulating xenon.

Glass pieces were cleaned in oxalic acid (1 %) on a hot plate (60-80 °C) and then in ethanol and acetone.

Then pieces were loaded into two crushers (1.6867 g and 0.9647g respectively) for noble gas analyses and baked at 100 °C for several days in order to remove weakly bonded atmospheric gases.

#### Step-crushing analyses

The two crushers were connected to the Helix SFT (ThermoScientific) vacuum line in the IPGP laboratory (Fig. S-8). Gases were extracted from samples in several crushing steps. For each step, the extracted gases were first purified successively on two titanium sponges (first at 800 °C for five minutes and then at ambient temperature during 10 minutes) to remove all reactive gases. After the double purification, Ar, Kr and Xe were trapped onto the activated charcoal trap 1 (Fig. S-8) at liquid nitrogen temperature. He and Ne were then analysed with the Helix SFT as described by Moreira *et al.* (2018).

If the $^{20}Ne/^{22}Ne$ ratio was higher than 11.8, then Ar, Kr and Xe trapped on the trap 1 were released from the trap and re-trapped on the trap 2 (Figure S-7). Otherwise, Ar, Kr and Xe were pumped. As shown in Figure S-1, this limit allows keeping non-contaminated xenon due to the curvature of the hyperbola, a plateau is reached for low $^{20}Ne/^{22}Ne$ values. However, this limit is too low for argon due to the inverse hyperbola curvature (Fig. S-1) and so argon should show more air contamination, which is the case (Table S-2).

In total, 22 crush steps were conducted and Ar, Kr and Xe were kept on trap 2 for 9 steps (trap 2 remained 25 days in static in total).

Then the setting with the two traps (Trap 1 and 2) was connected to the Noblesse (Nu Instruments) vacuum line for analysis of the accumulated Ar, Kr and Xe. Indeed, the xenon sensitivity on the Noblesse mass spectrometer (8.29 (± 0.35) x$10^{-16}$ cc/cps) is more than three times better than that of the Helix SFT. The accumulated gas was analysed the 37$^{th}$ day after starting the accumulation protocol. An air standard was used to calibrate sensitivities on the Noblesse mass spectrometer, of which a pipette of 0.410 $cm^3$ is taken from a 1 L reservoir each time. This air standard was prepared introducing 0.410 $cm^3$ of air in this 1 L reservoir.

As explained in Moreira *et al.* (2018), data are processed with our home-made software in Matlab©, which in particular allows to interpolate each isotope to the reference isotope for the elements that are analysed in peak-jumping mode (this is the case for Kr and Xe).

The measured accumulated Ar, Kr and Xe were corrected in Tables S-1 and S-2 for the line blank (the blank was less than 1 % for Ar, Kr and Xe). The data was not corrected for a blank of 37 days. But as discussed in the main text, the high $^{129}Xe/^{130}Xe$ ratio of 7.41 ± 0.03 (1σ) shows that the blank is very limited if one considered that the mantle $^{129}Xe/^{130}Xe$ ratio is 7.6, based on popping rock data (Moreira *et al.*, 1998) (Fig. S-1). To take into account this small atmospheric contamination, the measured xenon isotopic ratios were corrected by extrapolation to a $^{129}Xe/^{130}Xe$ ratio of 7.6 (Table S-1).

The new protocol to measure non-contaminated mantle xenon and krypton appears to be very efficient, since the $^{129}Xe/^{130}Xe$ ratio is very high and also because the new data fall on the same mixing line as defined by mantle-derived samples, among the highest values measured so far (Fig. S-2).

**Calculation of the $^{131-136}Xe/^{130}Xe$ ratios in the mantle before xenon recycling**

This calculation aims at determining a range for the fissiogenic xenon isotopic ratios ($^{131-132-134-136}Xe/^{130}Xe$) in the mantle before air recycling via subduction and a limit on the weighted average age of atmosphere recycling. This is complicated by the fact that the xenon isotopic composition of the atmosphere seems to have changed over time, becoming more enriched in heavy xenon isotopes compared to the starting composition (Pujol *et al.*, 2011; Avice *et al.*, 2017, 2018; Bekaert *et al.*, 2018).

We first used the power law suggested by Bekaert *et al.* (2018) to calculate the xenon isotopic ratios of the atmosphere through time.

Then, a Monte Carlo simulation is performed, consisting of first choosing a value for each isotopic ratio ($^{128-131-132-134-136}Xe/^{130}Xe$) in a μ ± 1σ space, where μ is the corrected data and σ the uncertainty (Table S-1).

The minimum ratios in the mantle before xenon recycling are calculated considering a mixing line passing through the present-day atmosphere and the corrected data. The minimum fissiogenic ratios $^{131-132-134-136}Xe/^{130}Xe$ are obtained by the intersection of this mixing line with the line of Phase Q (chondritic) for the $^{128}Xe/^{130}Xe$ ratio assuming the initial mantle was chondritic as suggested by the new data (Fig. 3 and Fig. S-7).

For deriving the maximum possible ratios in the mantle before xenon recycling, we also considered mixing lines passing through the corrected data and each previous atmospheric composition. As can be seen in Figure 3 and Figure S-7, if a very ancient air composition is taken (at 3.5 Gyr ago for example), the slope of the mixing line is negative, meaning that the initial $^{128}Xe/^{130}Xe$ ratio of the mantle would have been lower than the present-day value, which is not possible. So to calculate the maximum ratios, we considered the first possible mixing line with a positive slope and then the maximum ratios are obtained by the intersection of this mixing line with the line of Phase Q for the $^{128}Xe/^{130}Xe$ ratio (Fig. 3 and Fig. S-7). Hence, this calculation allows to constrain the limit on the weighted average age of atmosphere recycling, that is the earlier time where recycling of xenon started to be efficient. We excluded mixing lines with too small slope (< 0.001) giving unrealistically high $^{131-132-134-136}Xe/^{130}Xe$, but this does not influence the earlier time where effective recycling could have started. We also exclude realizations for which the fissiogenic xenon ratios ($^{131-134-136}Xe/^{132}Xe$) do not fall into the triangle defined by Phase Q, pure xenon from fission of $^{244}Pu$ and pure xenon from $^{238}U$ (Fig. S-9). A total of $10^5$ realizations were performed, which appear to be more than sufficient to get reproducible results. If only recycling of present-day air occurred, then the minimum $^{131-132-134-136}Xe/^{130}Xe$ ratios would be 5.6 ± 0.2, 8.0 ± 0.5, 4.0 ± 0.5 and 3.9 ± 0.6 (1σ) respectively. The maximum air-corrected mantle $^{131-132-134-136}Xe/^{130}Xe$ ratios are determined to be 10.8 ± 1.5, 22.8 ± 4.3, 19.4 ± 4.5 and 21.9 ± 5.2 (1σ), respectively (Fig. S-5 and S-6) for a recycling of air at 2.8 ± 0.3 (1σ) Gyr ago (Fig. 3 and Fig. S-7).

We note that the use of a power law can be debated. Indeed, if the evolution of the atmospheric xenon isotopic composition is due to xenon loss (Hébrard and Marty, 2014; Avice *et al.*, 2018; Zahnle *et al.*, 2019), similar to a Rayleigh distillation process, then an exponential law could be more appropriate. Hence, we also performed all the above calculations with the exponential law fitting U-Xe suggested by Bekaert *et al.* (2018). We found similar results, the maximum $^{131-132-134-136}Xe/^{130}Xe$ ratios being found are 10.7 ± 1.5, 22.6 ± 4.5, 19.1 ± 4.7 and 21.7 ± 5.5 (1σ) and the time for the start of volatile recycling efficiency is 3.2 ± 0.3 (1σ) Gyr ago.

## *Supplementary Tables*

**Table S-1** Xenon isotopic composition of popping rock 2πD43 analysed via the new protocol to accumulate non-contaminated, mantle xenon. For comparison, the air composition (Basford *et al.*, 1973) (used for the air standard) is indicated, as well as compositions for phase Q (Busemann *et al.*, 2000), the solar wind (Meshik *et al.*, 2014) and U-Xe (Pepin, 2000). Errors are 1 sigma uncertainties.

| | $^{130}$Xe x10$^{-12}$ ccSTP | $^{124}$Xe/$^{130}$Xe | $^{126}$Xe/$^{130}$Xe | $^{128}$Xe/$^{130}$Xe | $^{129}$Xe/$^{130}$Xe | $^{131}$Xe/$^{130}$Xe | $^{132}$Xe/$^{130}$Xe | $^{134}$Xe/$^{130}$Xe | $^{136}$Xe/$^{130}$Xe |
|---|---|---|---|---|---|---|---|---|---|
| 2πD43 | 1.78 | 0.0243 | 0.0226 | 0.478 | 7.41 | 5.28 | 6.84 | 2.81 | 2.47 |
| | 0.10 | 0.0006 | 0.0007 | 0.004 | 0.03 | 0.02 | 0.03 | 0.01 | 0.01 |
| 2πD43 corrected | | 0.0245 | 0.0228 | 0.4795 | 7.6 | 5.29 | 6.89 | 2.86 | 2.53 |
| | | 0.0007 | 0.0008 | 0.0048 | 0 | 0.02 | 0.04 | 0.02 | 0.02 |
| Air | | 0.0234 | 0.0218 | 0.471 | 6.50 | 5.21 | 6.61 | 2.56 | 2.18 |
| Phase Q | | 0.0281 | 0.0251 | 0.508 | 6.44 | 5.06 | 6.18 | 2.33 | 1.95 |
| Solar wind | | 0.0298 | 0.0252 | 0.510 | 6.31 | 5.00 | 6.06 | 2.24 | 1.82 |
| U-Xe | | 0.02928 | 0.02534 | 0.5083 | 6.286 | 4.996 | 6.047 | 2.126 | 1.657 |

**Table S-2** Argon and krypton isotopic compositions of popping rock 2πD43 analysed via the new protocol to accumulate non-contaminated, mantle gases. For comparison, the air composition (Nier, 1950; Basford *et al.*, 1973; Sano *et al.*, 2013) (used for the air standard) is indicated, as well as compositions for phase Q (Busemann *et al.*, 2000) and the solar wind (Meshik *et al.*, 2014). Errors are 1 sigma uncertainties.

| | $^{36}$Ar x10$^{-9}$ ccSTP | s | $^{38}$Ar/$^{36}$Ar | s | $^{40}$Ar/$^{36}$Ar | s | $^{84}$Kr x10$^{-10}$ ccSTP | s | $^{86}$Kr/$^{84}$Kr | s |
|---|---|---|---|---|---|---|---|---|---|---|
| 2πD43 | 4.52 | 0.07 | 0.1919 | 0.0006 | 15169 | 139 | 1.59 | 0.07 | 0.3059 | 0.0007 |
| 2πD43 (aliquot 2 for Ar only) | | | 0.1895 | 0.0004 | 16856 | 103 | | | | |
| Air | | | 0.1880 | | 295.5 | | | | 0.3052 | |
| Phase Q | | | 0.1873 | | | | | | 0.3095 | |
| Solar wind | | | 0.1814 | | | | | | 0.3012 | |

## *Supplementary Figures*

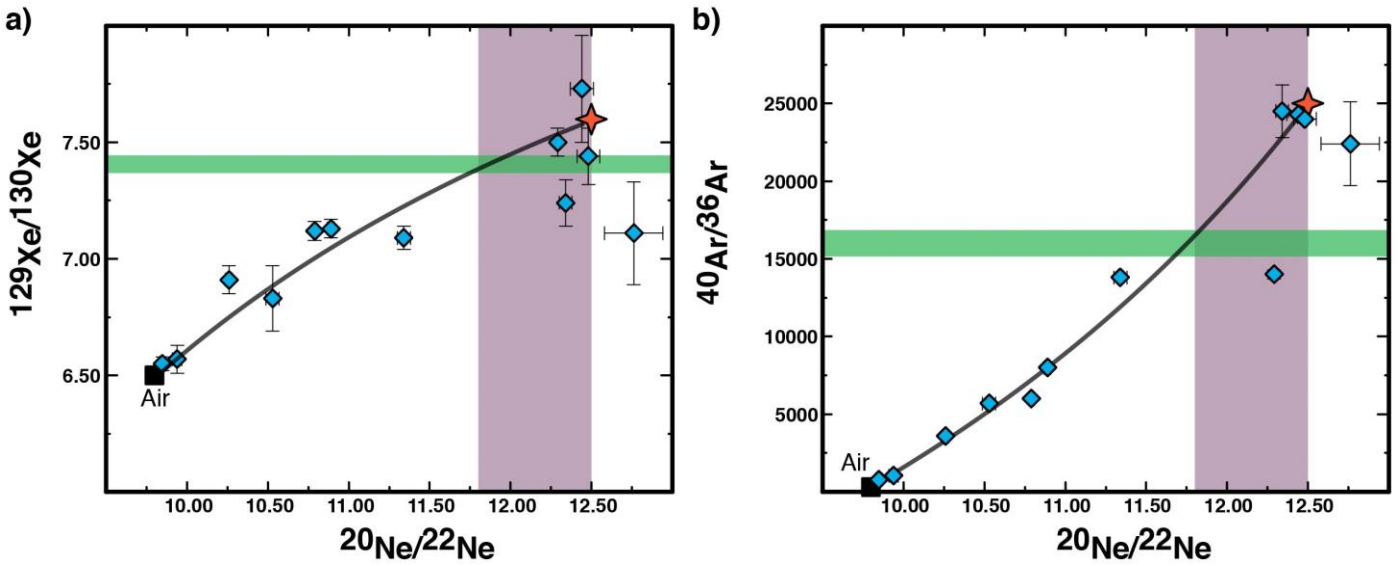


**Figure S-1** Correlation of **(a)** $^{129}Xe/^{130}Xe$ isotopic ratio and **(b)** $^{40}Ar/^{36}Ar$ isotopic ratio with the $^{20}Ne/^{22}Ne$ ratio for the popping rock 2πD43 (Moreira *et al.*, 1998). The orange star is the upper mantle composition (Moreira *et al.*, 1998). The pink areas show the $^{20}Ne/^{22}Ne$ range (11.8-12.5) for which Ar, Kr and Xe from crush steps were trapped. If the $^{20}Ne/^{22}Ne$ ratio of one crush step was lower than 11.8, Ar, Kr and Xe were pumped (see text). This $^{20}Ne/^{22}Ne$ range allows keeping only non-contaminated xenon but not for argon given the inverse hyperbola curvature. The green bars correspond to the measured $^{129}Xe/^{130}Xe$ and $^{40}Ar/^{36}Ar$ ratios for the accumulated gas from the popping rock 2πD43 (Tables S-1 and S-2).

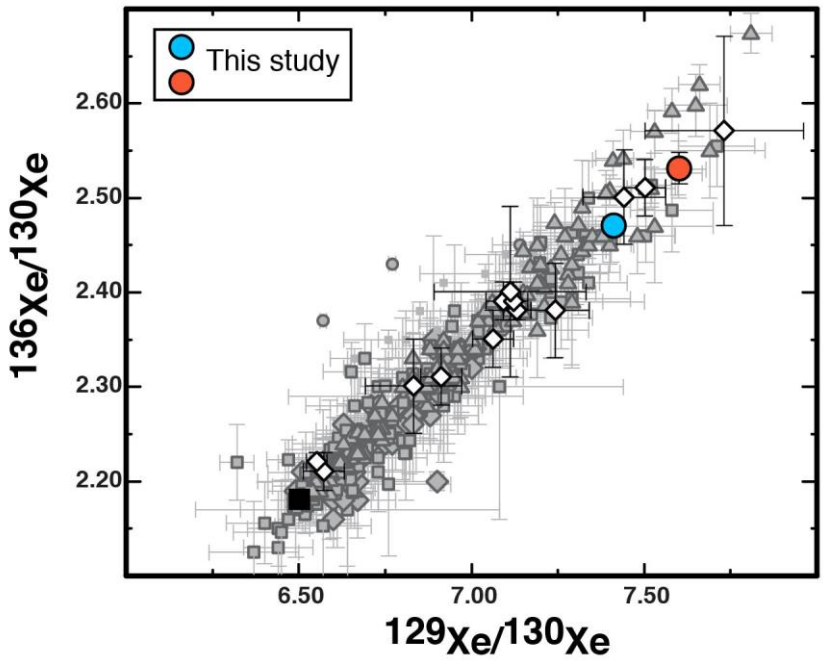


**Figure S-2** Compilation of xenon data for MORBs, OIBs, $CO_2$ well gases and thermal springs. Data from the literature for MORBs (Kunz *et al.*, 1998; Parai *et al.*, 2012; Tucker *et al.*, 2012; Parai and Mukhopadhyay, 2015), OIBs (Poreda and Farley, 1992; Trieloff *et al.*, 2000; Mukhopadhyay, 2012), $CO_2$ well gases and thermal springs (Caffee *et al.*, 1999; Holland and Ballentine, 2006; Holland *et al.*, 2009; Caracausi *et al.*, 2016; Moreira *et al.*, 2018) are in grey. Previous data for the popping rock 2πD43 are in open diamonds (Moreira *et al.*, 1998). The measured data with the new protocol is indicated with the blue circle and the corrected data with the orange circle. The new data fall on the same mixing line as previous data. Air (black square).

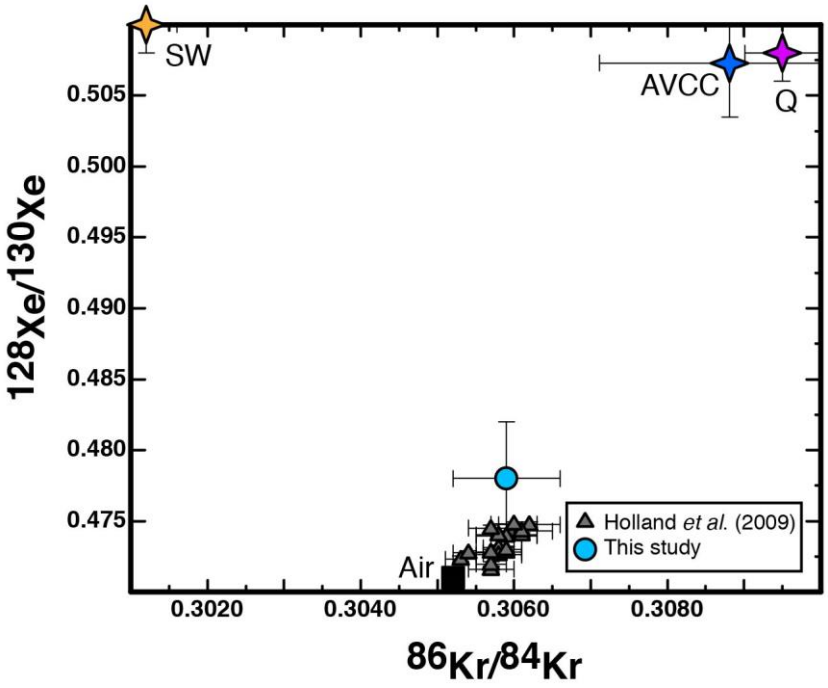


**Figure S-3** $^{86}Kr/^{84}Kr$ versus $^{128}Xe/^{130}Xe$ for popping rock 2πD43 (blue dot) analysed in this study. Data of Holland *et al.* (2009) (corrected for crustal uranium fission, grey triangles) are also shown with the composition of phase Q (Busemann *et al.*, 2000)., the solar wind (Meshik *et al.*, 2014) and AVCC for Average Carbonaceous chondrites (Pepin, 2003).

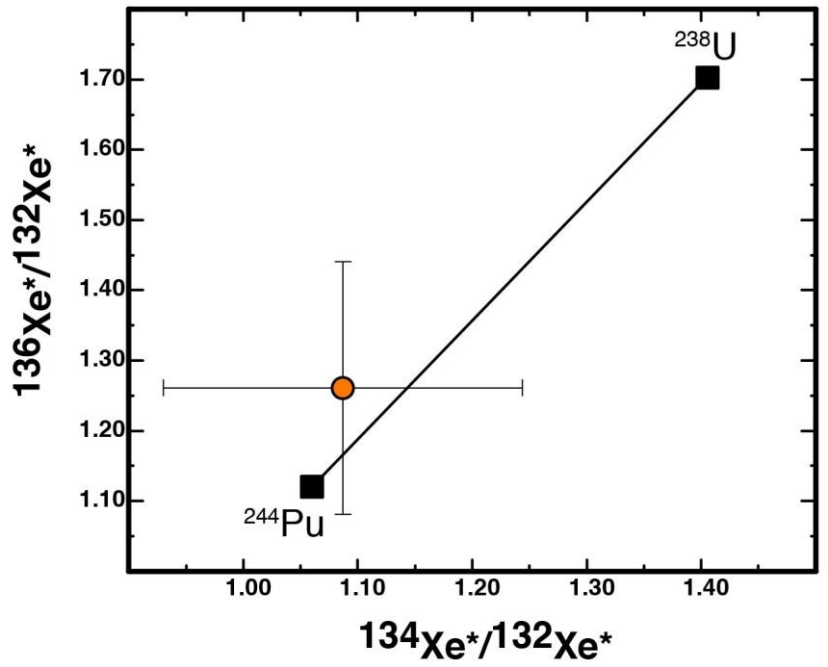


**Figure S-4** Excess of fissiogenic xenon in sample 2πD43 to present-day air. The orange dot is obtained from the popping rock data corrected for atmospheric contamination (see method in Moreira, 2013). The fissiogenic xenon in the 2πD43 source shows more Pu-derived xenon contribution than uranium-derived xenon, contrary to other MORBs data (Tucker *et al.*, 2012; Parai and Mukhopadhyay, 2015).

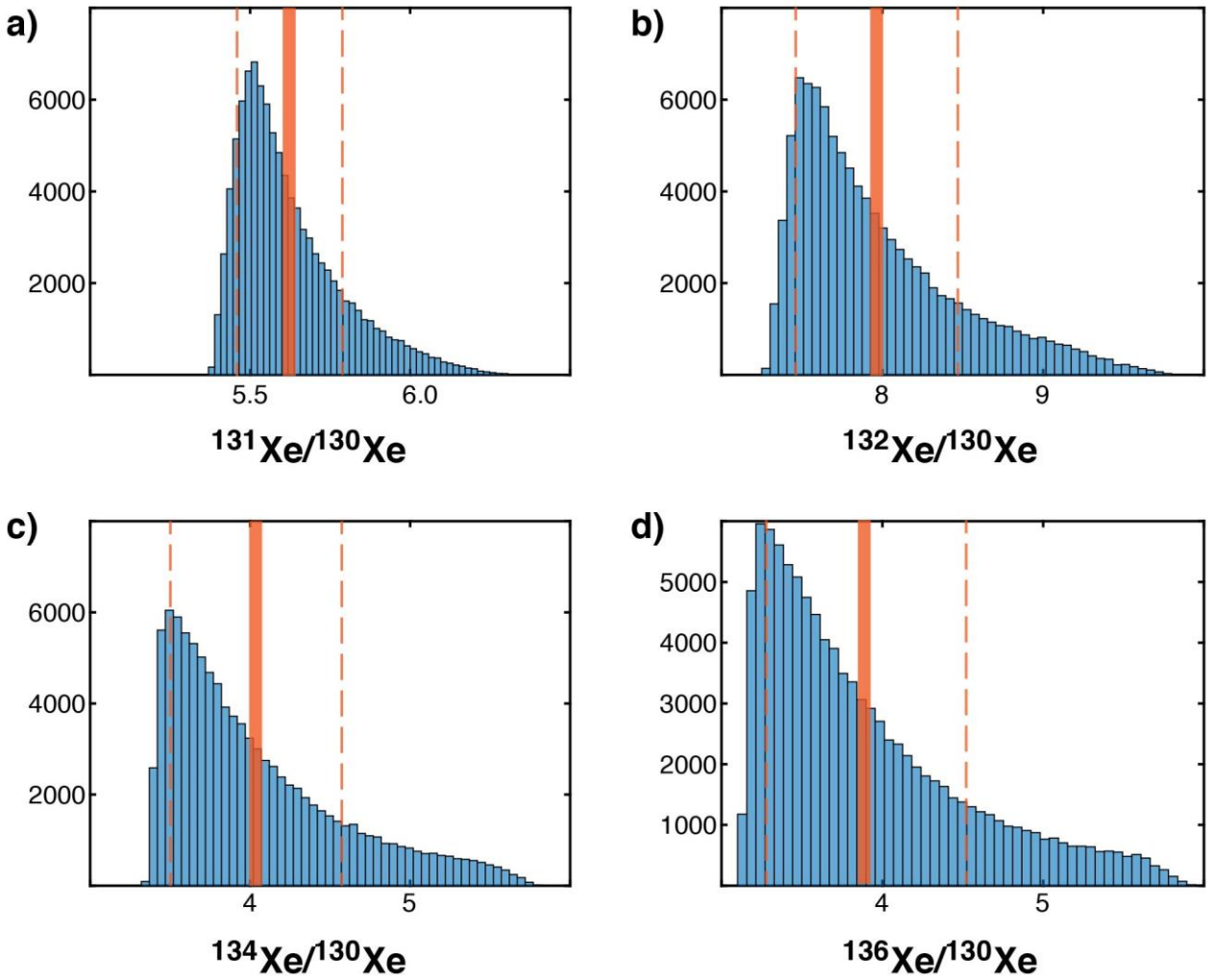


**Figure S-5** Histograms of the Monte Carlo simulations to determine the minimum $^{131\text{-}132\text{-}134\text{-}136}Xe/^{130}Xe$ ratios in the mantle before atmospheric xenon recycling. The orange bars show the mean values and the orange dotted lines the 1 sigma uncertainties.

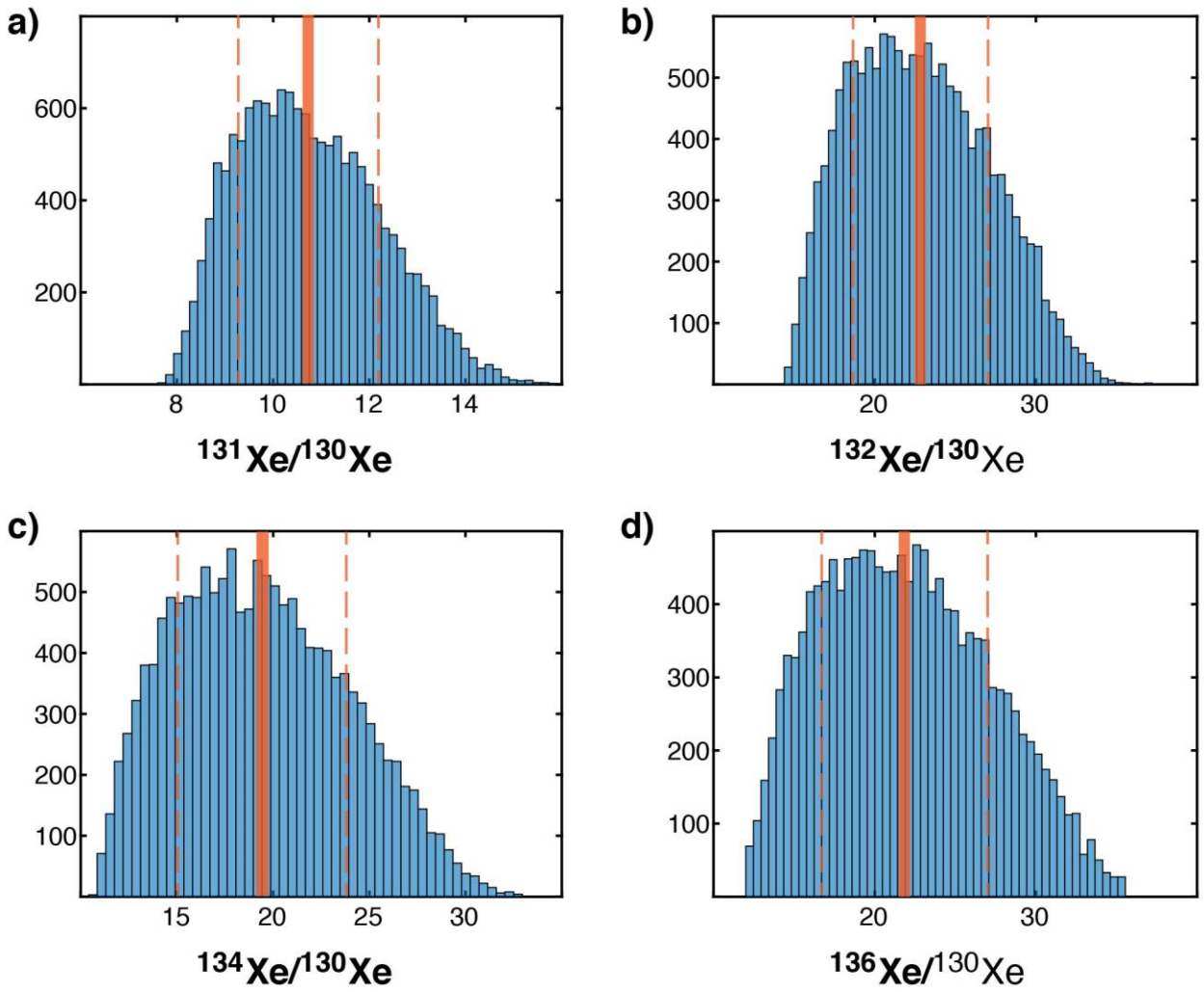


**Figure S-6** Histograms of the Monte Carlo simulations to determine the maximum $^{131\text{-}132\text{-}134\text{-}136}Xe/^{130}Xe$ ratios in the mantle before atmospheric xenon recycling. The orange bars show the mean values and the orange dotted lines the 1 sigma uncertainties.

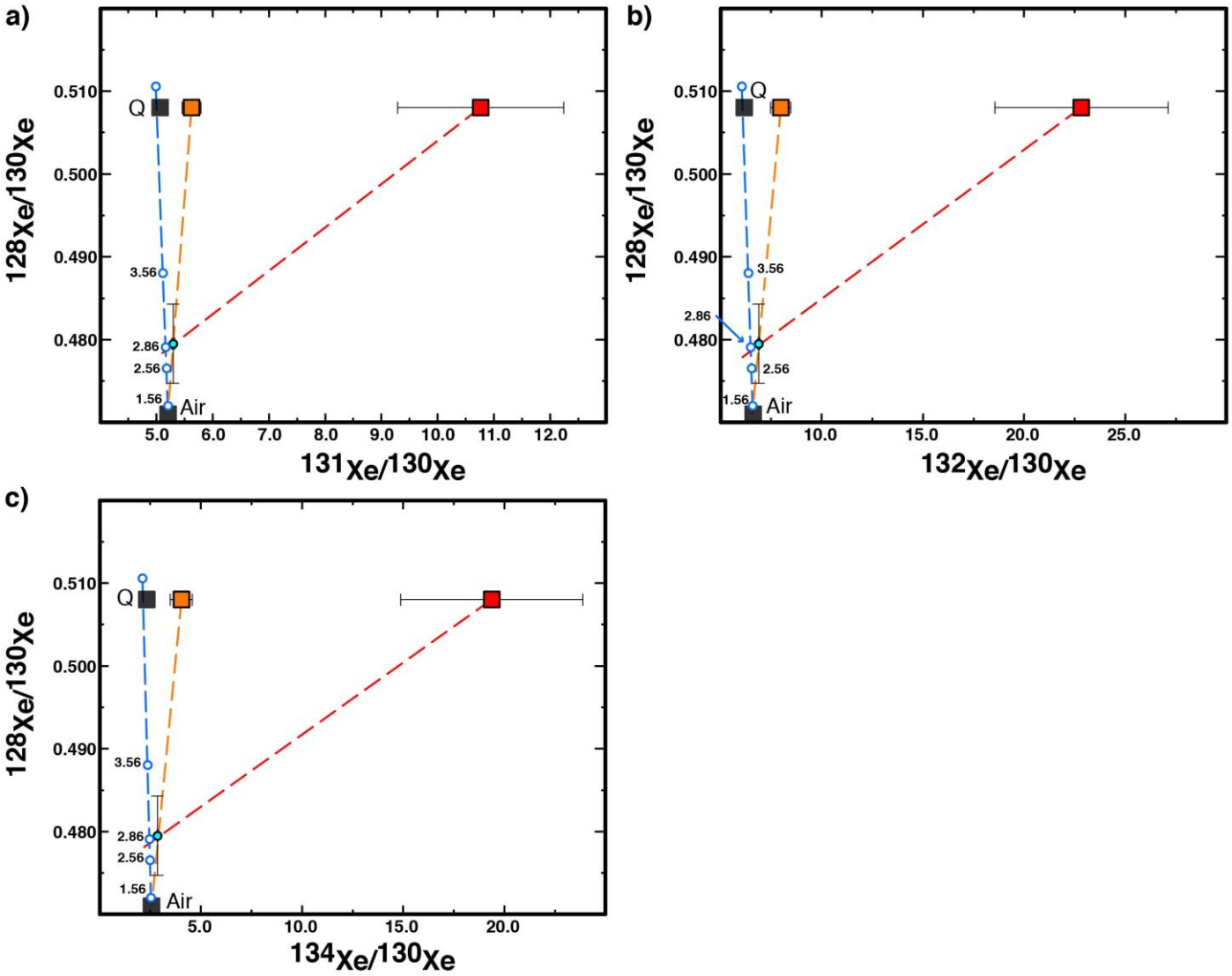


**Figure S-7** Determination of the mantle xenon isotopic ratios before recycling. The evolution of the xenon atmospheric composition is represented with the blue dots and blue dotted lines with the numbers indicating the time in Gyr (a power law was considered (Bekaert *et al.*, 2018)): **(a)** for the $^{131}Xe/^{130}Xe$ ratio, **(b)** for the $^{132}Xe/^{130}Xe$ ratio and **(c)** for the $^{134}Xe/^{130}Xe$ ratio. The corrected data for shallow atmospheric contamination is shown (light blue dot). The minimum (orange square) and maximum (red square) $^{131\text{-}132\text{-}134}Xe/^{130}Xe$ ratios in the mantle before recycling of atmospheric xenon are calculated considering mixing with air (orange and red dotted lines) and that the initial $^{128}Xe/^{130}Xe$ is chondritic (Phase Q). The red lines suggest that recycling of atmospheric xenon could have been effective only since 2.8 ± 0.3 (1σ) Gyr ago (see text). Otherwise, unreasonable values of $^{131\text{-}132\text{-}134\text{-}136}Xe/^{130}Xe$ ratios are obtained. Phase Q (Busemann *et al.*, 2000).

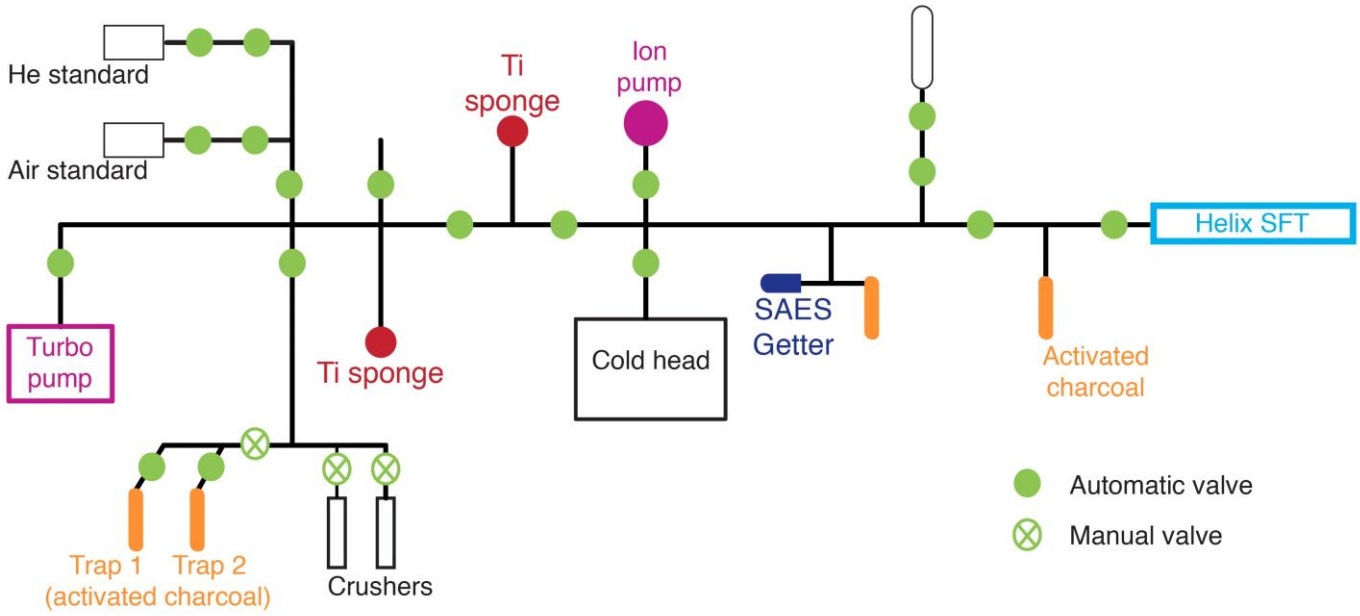


**Figure S-8** Schematic view of the vacuum line connected to the Helix SFT mass spectrometer (ThermoScientific).

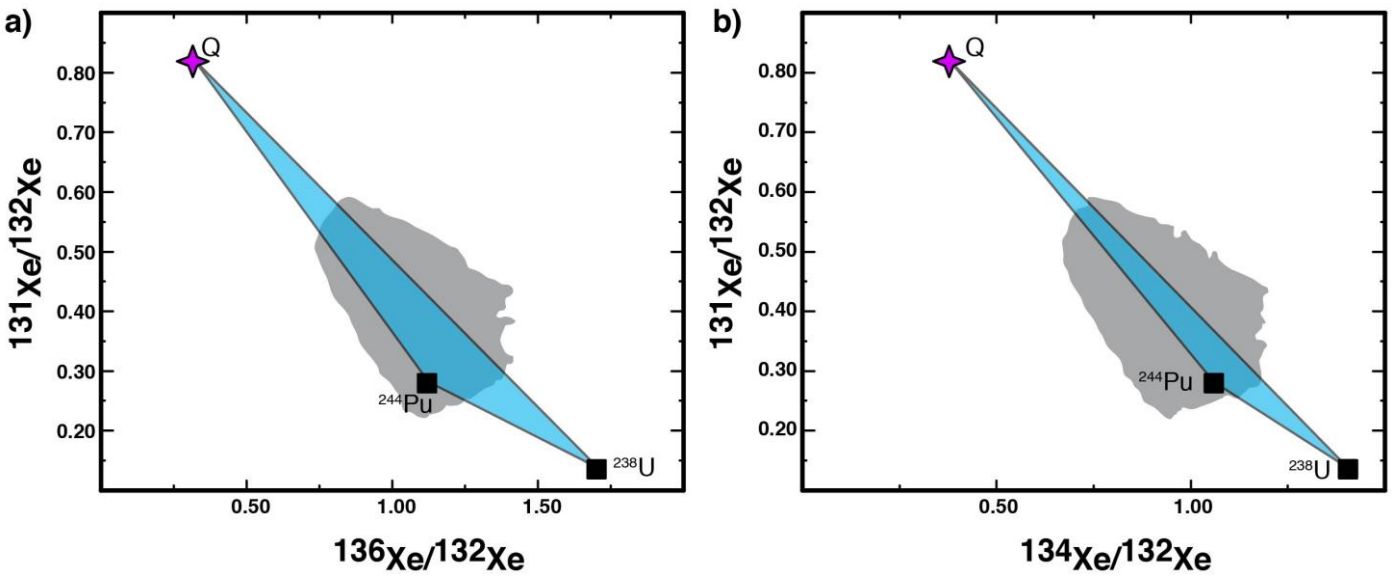


**Figure S-9** Heavy xenon fissiogenic isotopes plot. The calculated maximum $^{131\text{-}132\text{-}134\text{-}136}$Xe/$^{130}$Xe ratios of all the realizations fall in the grey areas. Only calculated maximum $^{131\text{-}132\text{-}134\text{-}136}$Xe/$^{130}$Xe ratios that fall into the blue triangles, defined by Phase Q (Busemann *et al.*, 2000), pure xenon from fission of $^{244}$Pu and pure xenon from fission of $^{238}$U, are considered.

## *Supplementary Information References*


Avice, G., Marty, B., Burgess, R. (2017) The origin and degassing history of the Earth's atmosphere revealed by Archean xenon. *Nature Communications* 8, 15455.

Avice, G., Marty, B., Burgess, R., Hofmann, A., Philippot, P., Zahnle, K., Zakharov, D. (2018) Evolution of atmospheric xenon and other noble gases inferred from Archean to Paleoproterozoic rocks. *Geochimica et Cosmochimica Acta* 232, 82-100.

Basford, J.R., Dragon, J.C., Pepin, R.O., Coscio, M.R.J., Murthy, V.R. (1973) Krypton and xenon in lunar fines. In: Gose, W.A. (Ed.) *Fourth Lunar Science Conference*. Pergamon Press, Houston,Tx, 53.

Bekaert, D.V., Broadley, M.W., Delarue, F., Avice, G., Robert, F., Marty, B. (2018) Archean kerogen as a new tracer of atmospheric evolution: Implications for dating the widespread nature of early life. *Science Advances* 4, doi: 10.1126/sciadv.aar2091.

Bougault, H., Dmitriev, L., Schilling, J.-G., Sobolev, A., Joron, J.-L., Needham, H.D. (1988) Mantle heterogeneity from trace elements: MAR triple junction near 14°N. *Earth and Planetary Science Letters* 88, 27-36.

Busemann, H., Baur, H., Wieler, R. (2000) Primordial noble gases in "phase Q" in carbonaceous and ordinary chondrites studied by closed-system stepped etching. *Meteor. and Planet. Science* 35, 949-973.

Caffee, M.W., Hudson, G.P., Velsko, C., Huss, G.R., Alexander, E.C., Chivas, R. (1999) Primordial Noble Gases from Earth's Mantle: Identification of Primitive Volatile Component. *Science* 285, 2115-2118.

Caracausi, A., Avice, G., Burnard, P.G., Füri, E., Marty, B. (2016) Chondritic xenon in the Earth's mantle. *Nature* 533, 82-85.

Hébrard, E., Marty, B. (2014) Coupled noble gas–hydrocarbon evolution of the early Earth atmosphere upon solar UV irradiation. *Earth and Planetary Science Letters* 385, 40-48.

Holland, G., Ballentine, C.J. (2006) Seawater subduction controls the heavy noble gas composition of the mantle. *Nature* 441, 186-191.

Holland, G., Cassidy, M., Ballentine, C.J. (2009) Meteorite Kr in Earth's Mantle Suggests a Late Accretionary Source for the Atmosphere. *Science* 326, 1522-1525.

Javoy, M., Pineau, F. (1991) The volatiles record of a « popping » rock from the Mid-Atlantic Ridge at 14°N : chemical and isotopic composition of gas trapped in the vesicles. *Earth and Planetary Science Letters* 107, 598-611.

Kunz, J., Staudacher, T., Allègre, C.J. (1998) Plutonium-Fission Xenon Found in Earth's Mantle. *Science* 280, 877-880.

Meshik, A., Hohenberg, C., Pravdivtseva, O., Burnett, D. (2014) Heavy noble gases in solar wind delivered by Genesis mission. *Geochimica et Cosmochimica Acta* 127, 326-347.

Moreira, M. (2013) Noble gas constraints on the origin and evolution of Earth's volatiles. *Geochemical Perspectives* 2, 229-403.

Moreira, M., Kunz, J., Allègre, C.J. (1998) Rare gas systematics on popping rock : estimates of isotopic and elemental compositions in the upper mantle. *Science* 279, 1178-1181.

Moreira, M., Rouchon, V., Muller, E., Noirez, S. (2018) The xenon isotopic signature of the mantle beneath Massif Central. *Geochemical Perspectives Letters* 6, 28-32.

Mukhopadhyay, S. (2012) Early differentiation and volatile accretion recorded in deep mantle Neon and Xenon. *Nature* 486, 101-104.

Nier, A.O. (1950) A Redetermination of the Relative Abundances of the Isotopes of Carbon, Nitrogen, Oxygen, Argon, and Potassium. *Physical Review* 77, 789-793.

Parai, R., Mukhopadhyay, S. (2015) The evolution of MORB and plume mantle volatile budgets: Constraints from fission Xe isotopes in Southwest Indian Ridge basalts. *Geochemistry, Geophysics, Geosystems* 16, 719-735.

Parai, R., Mukhopadhyay, S., Standish, J.J. (2012) Heterogeneous upper mantle Ne, Ar and Xe isotopic compositions and a possible Dupal noble gas signature recorded in basalts from the Southwest Indian Ridge. *Earth and Planetary Science Letters* 359-360, 227-239.

Pepin, R.O. (2000) On the Isotopic Composition of Primordial Xenon in Terrestrial Planet Atmospheres. *Space Science Reviews* 92, 371-395.

Pepin, R.O. (2003) On Noble Gas Processing in the Solar Accretion Disk. *Space Science Reviews* 106, 211-230.

Poreda, R.J., Farley, K.A. (1992) Rare gases in Samoan xenoliths. *Earth and Planetary Science Letters* 113, 129-144.

Pujol, M., Marty, B., Burgess, R. (2011) Chondritic-like xenon trapped in Archean rocks: A possible signature of the ancient atmosphere. *Earth and Planetary Science Letters* 308, 298-306.

Sano, Y., Marty, B., Burnard, P. (2013) Noble Gases in the Atmosphere. In: Burnard, P. (Ed.) *The Noble Gases as Geochemical Tracers*. Springer Berlin Heidelberg, 17-31.

Sarda, P., Graham, D.W. (1990) Mid-ocean ridge popping rocks: implications for degassing at ridge crests. *Earth and Planetary Science Letters* 97, 268-289.

Trieloff, M., Kunz, J., Clague, D.A., Harrison, D., Allègre, C.J. (2000) The Nature of pristine noble gases in mantle plumes. *Science* 288, 1036-1038.

Tucker, J.M., Mukhopadhyay, S., Schilling, J.-G. (2012) The heavy noble gas composition of the depleted MORB mantle (DMM) and its implications for the preservation of heterogeneities in the mantle. *Earth and Planetary Science Letters* 355-356, 244-254.

Zahnle, K.J., Gacesa, M., Catling, D.C. (2019) Strange messenger: A new history of hydrogen on Earth, as told by Xenon. *Geochimica et Cosmochimica Acta* 244, 56-85.